Turbulence is an Ineffective Mixer when Schmidt Numbers Are Large

Dhawal Buaria[,1,*] Matthew P. Clay[,2] Katepalli R. Sreenivasan[,1,3] and P. K. Yeung[2,4]

[1]*Tandon School of Engineering, New York University, New York, New York 11201, USA*
[2]*School of Aerospace Engineering, Georgia Institute of Technology, Atlanta, Georgia 30332, USA*
[3]*Department of Physics and the Courant Institute of Mathematical Sciences, New York University,
New York, New York 10012, USA*
[4]*School of Mechanical Engineering, Georgia Institute of Technology, Atlanta, Georgia 30332, USA*

We solve the advection-diffusion equation for a stochastically stationary passive scalar θ, in conjunction with forced 3D Navier-Stokes equations, using direct numerical simulations in periodic domains of various sizes, the largest being 8192^3. The Taylor-scale Reynolds number varies in the range 140–650 and the Schmidt number $\mathrm{Sc} \equiv \nu/D$ in the range 1–512, where ν is the kinematic viscosity of the fluid and D is the molecular diffusivity of θ. Our results show that turbulence becomes an ineffective mixer when Sc is large. First, the mean scalar dissipation rate $\langle\chi\rangle = 2D\langle|\nabla\theta|^2\rangle$, when suitably nondimensionalized, decreases as $1/\log \mathrm{Sc}$. Second, 1D cuts through the scalar field indicate increasing density of sharp fronts on larger scales, oscillating with large excursions leading to reduced mixing, and additionally suggesting weakening of scalar variance flux across the scales. The scaling exponents of the scalar structure functions in the inertial-convective range appear to saturate with respect to the moment order and the saturation exponent approaches unity as Sc increases, qualitatively consistent with 1D cuts of the scalar.

Introduction—A defining property of fluid turbulence, which plays a critical role in myriad natural and engineering processes, is that it mixes substances extremely well [1–3]. Thus, any circumstances in which turbulence loses that property is naturally important to study and understand. This Letter examines such an instance by considering mixing of passive scalars with large Schmidt numbers, $\mathrm{Sc} \equiv \nu/D$, where ν is the kinematic viscosity of the fluid and D is the molecular diffusivity of the mixing substance. By analyzing a massive database generated through state-of-the-art direct numerical simulations (DNS) of the governing equations, we show that even fully developed turbulence at high Reynolds number becomes an ineffective mixer when the Sc is rendered large.

The rate of mixing of a scalar θ is related to the average "dissipation" rate $\langle\chi\rangle$ of its variance, defined as $\langle\chi\rangle = 2D\langle|\nabla\theta|^2\rangle$. There is a general claim that $\langle\chi\rangle$ remains finite even when $D \to 0$. This claim derives from the analogy with the mean dissipation rate of turbulent kinetic energy, which is theorized to be independent of viscosity when the latter is sufficiently small ($\nu \to 0$) [4,5]. There is concrete empirical evidence that anomalous dissipation of kinetic energy is essentially correct [6–9]. However, whether the analogous property holds for scalar dissipation still remains an unresolved question [10–13]. We show that it does not when Sc is large.

Since the passive scalar is advected by the underlying velocity field, investigating scalar dissipation anomaly in principle requires the joint limit of $\nu, D \to 0$. Specific practical circumstances on how they approach zero, motivate two separate scenarios. In the first scenario, we can take the joint limit such that Sc is a constant and thus the Reynolds number increases. For this case, there is some evidence at $\mathrm{Sc} = \mathcal{O}(1)$ that the scalar dissipation indeed becomes independent of D [13]. Figure 1 reaffirms this by showing that $\langle\chi\rangle$, nondimensionalized by the large-scale
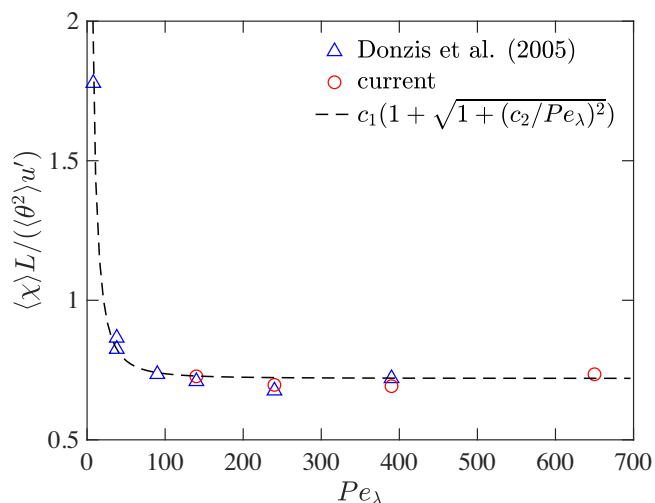

FIG. 1. Normalized scalar dissipation rate for $\mathrm{Sc} = 1$, as a function of microscale Péclet number $\mathrm{Pe}_\lambda \propto 1/D$. The data in (blue) triangles are from [13]; the new data are described in Table I. The functional form of the fit to the data in [13] is shown in the legend, with $c_1 = 0.36$ and $c_2 = 31$.

TABLE I.   Simulation parameters for the DNS runs used in the current work: the Taylor-scale Reynolds number R_λ, the Schmidt number Sc, the number of grid points for the velocity and scalar fields, N_v^3 and N_θ^3, the spatial resolution for the velocity and scalar fields, respectively $k_{\max}\eta$ and $k_{\max}\eta_B$, and the simulation length T_{sim} in statistically stationary state in terms of the large-eddy turnover time T_E. For each case, the domain length is $L_0 = 2\pi$, and $L \approx L_0/6$.

R_λ	Sc	N_v^3	$k_{\max}\eta$	N_θ^3	$k_{\max}\eta_B$	T_{sim}/T_E
140	1	512^3	3	512^3	3	10
140	4	512^3	3	1024^3	3	90
140	4	512^3	3	2048^3	6	27
140	8	256^3	1.5	1024^3	2	90
140	8	512^3	3	1024^3	2	85
140	8	512^3	3	2048^3	4	45
140	16	256^3	1.5	1024^3	1.5	98
140	16	256^3	1.5	2048^3	3	44
140	16	512^3	3	1024^3	1.5	84
140	16	512^3	3	2048^3	3	56
140	32	512^3	3	2048^3	2	44
140	32	512^3	3	2048^3	2	19
140	32	1024^3	6	4096^3	4	11
140	64	512^3	3	2048^3	1.5	53
140	64	1024^3	6	4096^3	3	9
140	128	512^3	3	4096^3	2	23
140	256	1024^3	6	8192^3	3	6
140	512	1024^3	6	8192^3	2	9
240	1	1024^3	3	1024^3	3	10
390	1	2048^3	3	2048^3	3	10
390	8	2048^3	3	8192^3	4	6
650	1	4096^3	3	4096^3	3	10

quantity $\langle\theta^2\rangle u'/L$, asymptotes to a constant for large Taylor-scale Péclet number $\text{Pe}_\lambda = u'\lambda/D$, where u' is the rms of velocity fluctuations, $\lambda = u'/\sqrt{\langle(\partial u/\partial x)^2\rangle}$ is the Taylor microscale, and L is the integral length scale.

In the second scenario, either ν or D approaches zero faster, such that the Sc $\to 0$ or ∞, respectively. Here, we focus on the latter case of Sc $\to \infty$ [14]. The mixing of scalars with Sc $\gg 1$ is characterized by the development of very fine scales, even smaller than those in the velocity field, which are extremely challenging to resolve in both experiments and simulations [15,16]. Consequently, the study of high Sc scalars has been historically limited to very low Reynolds numbers, where the turbulence is not adequately developed. However, even at very low Reynolds numbers, there has been some indication that the asymptotically constant values of $(\langle\chi\rangle L)/(\langle\theta^2\rangle u')$ become smaller with increasing Sc [13]. In this Letter, utilizing new state-of-the-art simulations at significantly higher Reynolds numbers (corresponding to fully developed turbulence), we present new results which demonstrate conclusively that the normalized scalar dissipation rate approaches zero at large Sc, rendering turbulence ineffective at mixing. We additionally show that this
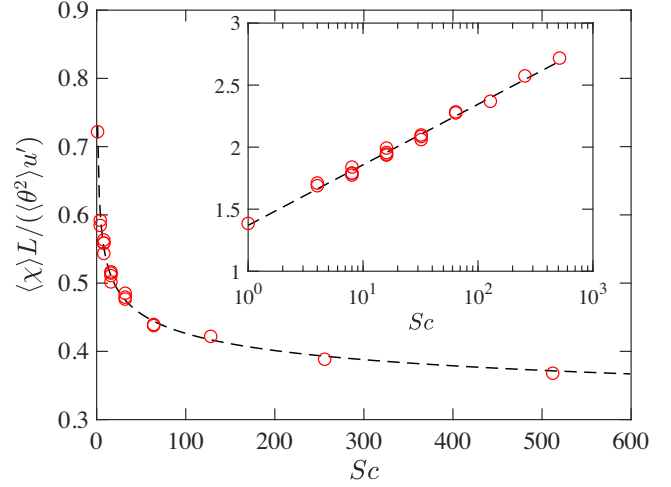

FIG. 2.   Test for scalar dissipation anomaly at $R_\lambda = 140$ with increasing Sc. The mean scalar dissipation rate is normalized as in Fig. 1. The dashed line corresponds to $1/\log \text{Sc}$ dependence. The inset shows the inverse of these data versus Sc on log-linear axes, affirming the $\log \text{Sc}$ dependence.

inefficacy is also carried over to the larger scales, with important theoretical and practical implications.

Direct numerical simulations.—The data utilized here are generated using the canonical DNS setup of isotropic turbulence in a periodic domain [17,18], forced at large scales to maintain statistical stationarity. For the passive scalar, we simultaneously solve the advection-diffusion equation in the presence of uniform mean-gradient $\nabla\Theta = (G, 0, 0)$ along the Cartesian direction x [19]. For Sc = 1, we utilize the conventional Fourier pseudospectral methods for both the velocity and scalar fields. For Sc = 4 and higher, we utilize a hybrid approach [20–22], where the velocity field is obtained pseudospectrally, focused on resolving the Kolmogorov length scale η, and the scalar field by using compact finite differences on a finer grid to adequately resolve the smaller Batchelor scale $\eta_B = \eta\text{Sc}^{-1/2}$ [23]. The database is summarized in Table I. For many cases, we have performed simulations with various small-scale resolutions to ensure accuracy of the statistics [24]. Our runs also meet the resolution requirements proposed in [25]. However, we note that while [25] was focused on studying extreme events, the statistics reported in this work are not as sensitive to resolution [26,27].

Reduction of mixing at diffusive scales.—Here, we explore the influence of Sc on mean scalar dissipation rate $\langle\chi\rangle$. We see in Fig. 2 that the asymptotic value of scalar dissipation continually decreases with Sc. In fact, using arguments based on functional form of the scalar spectrum, the authors of Refs. [13,28] showed that the inverse scalar dissipation rate $(\langle\theta^2\rangle u')/(\langle\chi\rangle L)$ varies as $\log \text{Sc}$. In order to see this behavior clearly, we plot the inverse dissipation

versus log Sc in the inset of Fig. 2. The data are in excellent agreement with expectations.

The observation that the normalized scalar dissipation tends to zero in the limit Sc → ∞, albeit logarithmically, suggests that the diffusivity is ultimately incapable of smoothing the scalar fluctuations and that there is no mixing at small scales. This picture can be intuitively understood from a Lagrangian perspective by considering trajectories of individual scalar particles [29–31]. Physically, mixing occurs when some local concentration of scalar particles eventually disperses through the fluid under the combined action of turbulence and molecular diffusion. If we consider two coincident scalar particles, the diffusivity is necessary to create some finite separation, thereafter allowing turbulence to take over; however, in the limit of $D \to 0$, they cannot separate and the action of turbulence does not manifest [32,33].

Reduced mixing at larger scales.—Figure 3 shows typical 1D cuts of the scalar field in the direction of the mean gradient. The upper panel corresponds to Sc = 1 and increasing R_λ. The well known ramp-cliff structures (see [34–37]) are clearly visible in all traces, with disorganized small-scale fluctuations superimposed on them. With increasing R_λ, small-scale fluctuations expectedly become more conspicuous, but the steep cliffs remain. In the lower panel, the cuts are for $R_\lambda = 140$ but varying Sc. For low to moderate Sc, the ramp-cliff structures stand out as before, but the superimposed scalar fluctuations become stronger with increasing Sc. The large-scale ramp-cliff structures seemingly continue to be present even at the highest Sc (= 512), but are overwhelmed by sharp oscillations essentially between the smallest and largest concentrations, leading to inefficient mixing at larger scales.

It is worth noting that the scalar dissipation also represents the scalar variance flux from the large scales through intermediate (inertial) scales to the smallest (analogous to the energy dissipation representing the flux of kinetic energy). Since the inertial range dynamics are not influenced by either ν or D, in principle the dimensional scalar dissipation can still be nonzero as Sc increases. However, in contrast the scalar variance increases with Sc (ostensibly through a broadening viscous-convective range), and thus causes the normalized scalar dissipation to approach zero. In other words, as Sc is increased, turbulence responds not only by producing strong scalar gradients, but even stronger scalar fluctuations, which ultimately lead to inefficient mixing.

Structure functions.—To further analyze the reduction in mixing, we consider the scalar increment $\Delta_r\theta$ between two points separated by distance r, whose moments are the scalar structure functions. In the so-called inertial-convective range, the pth order structure function is expected to follow a power law of the form $\langle (\Delta_r\theta)^p \rangle \sim r^{\zeta_p}$, where ζ_p is anomalous with
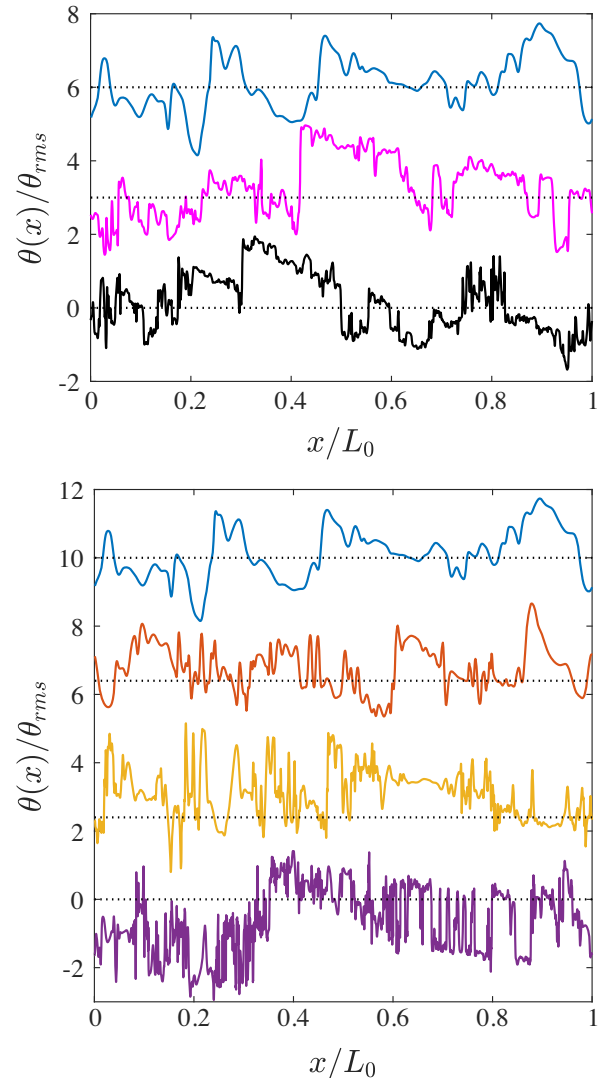

FIG. 3. Typical one-dimensional cuts of the scalar field, normalized by the rms, in the direction of the imposed mean gradient (x). $L_0 = 2\pi$ is the domain length. The curves in the upper panel correspond to fixed Sc = 1 and $R_\lambda = 140$, 390, and 650 from top to bottom; those in the lower panel are for fixed $R_\lambda = 140$ and Sc = 1, 8, 64, and 512 from top to bottom. The curves are shifted for clarity, as indicated by dotted horizontal lines.

respect to the Kolmogorov phenomenology (i.e., $\zeta_p = p/3$) [2,11,38]. In order to extract ζ_p, we have followed an analysis similar to the recent work [26] where ζ_2 was obtained by a power law fit in the inertial-convective range, and higher order moments were extracted through extended self-similarity [39].

The scaling exponents ζ_p are plotted against the moment order in Fig. 4, for $R_\lambda \geq 390$. The results for $R_\lambda = 650$ and Sc = 1 are virtually identical to those of [26], and reaffirm that the scalar exponents saturate to $\lim_{p\to\infty} \zeta_p = \zeta_\infty \approx 1.2$. In comparison, the exponents for $R_\lambda = 390$ and Sc = 1 are mostly identical to those at $R_\lambda = 650$, but differ somewhat
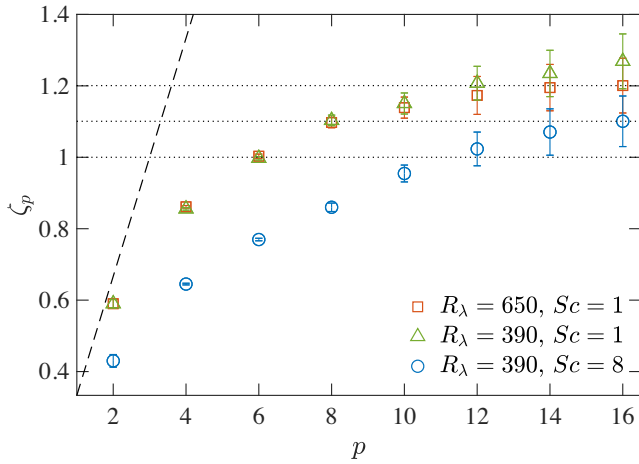
FIG. 4. The scalar increment exponent ζ_p as a function of the moment order p for R_λ and Sc shown in the legend. The error bars indicate 95% confidence interval. The dotted lines at 1.2 and 1.1 correspond to plausible saturation values at Sc = 1, 8, whereas the dotted line at 1 is the likely saturation value at Sc → ∞. The dashed line $\zeta_p = p/3$ corresponds to the Kolmogorov phenomenology.

for $p \geq 12$ (possibly due to a slightly smaller scaling range from which the exponents were extracted). The more important result is that for $R_\lambda = 390$ and Sc = 8 the exponents are consistently smaller than those for Sc = 1 and tend to saturate at a smaller value of $\zeta_\infty \approx 1.1$. Evidently, the smaller saturation value for larger Sc invites the question as to whether it is bounded as Sc → ∞.

For a definitive answer, one needs to obtain data for higher Sc for at least $R_\lambda = 650$ (at which convincing scaling exists). But large Sc at $R_\lambda = 650$ are unlikely to be attainable anytime soon. We have therefore analyzed the data at lower $R_\lambda = 140$, for which inertial range characteristics just begin to manifest [17,40]. In Fig. 5, we show the local slope of the structure functions for orders $p = 4, 8, 12$, and 16 at Sc = 32, 128, and 512 (the curves for different p are shifted for clarity). With increasing p, the curves for all Sc progressively get closer to local slope of unity. If we focus on the region $r/\eta \gtrsim 30$, which nominally corresponds to onset of the inertial-convective range [26], it appears that the local slope for all Sc are approximately equal for highest p values, and close to unity—hinting that the high-order exponents saturate at about 1 as Sc → ∞.

Codimension result.—Finally, we turn to quantifying the fractal dimension of sharp scalar fronts and understanding how it relates to the saturation exponent. In [26], the authors found that ζ_∞ and the box-counting dimension D_F of the sharp scalar fronts (satisfying the threshold $|\partial\theta/\partial x| \geq 0.2\theta_{\rm rms}/\eta_B$), add up to the Euclidean dimension of the flow, i.e., $\zeta_\infty + D_F = 3$. In that same spirit, we perform box counting of the strong scalar gradients corresponding to sharp fronts, given by $N(r)$ for various cubes of edge size r. For the saturation exponent $\zeta_\infty = 1$, the codimension corresponds to $D_F = 2$. In Fig. 6, we plot $N(r)/N^3$ compensated by r^{D_F} with $D_F = 2$, for the same cases shown in Fig. 5. Remarkably, the curves at the highest Sc exhibit an extended plateau for small scales, consistent with a fractal dimension of 2. For large r, all curves are consistent with $D_F = 3$, as expected by the space filling nature at large scales. This consolidates the result that
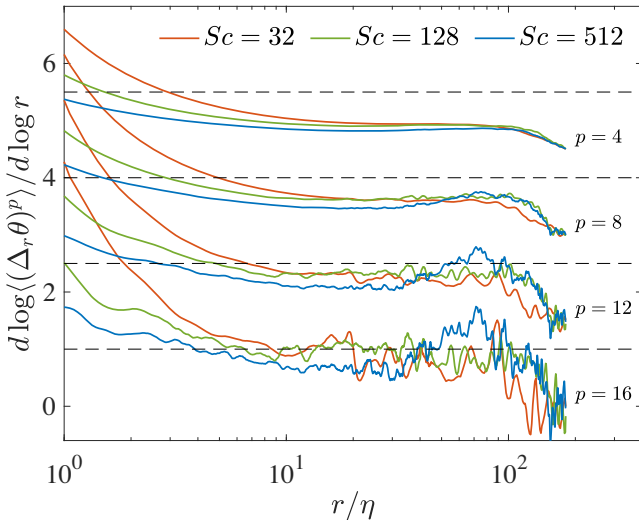

FIG. 5. The local slope of pth order scalar structure functions at $R_\lambda = 140$ and Sc = 32, 128, and 512. The curves are shown for $p = 4, 8, 12$, and 16. They are shifted vertically for clarity and the corresponding dashed lines represent a local slope of unity.
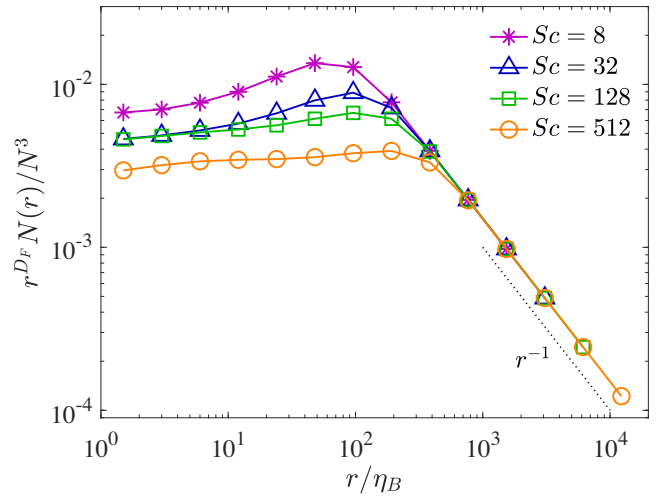

FIG. 6. Compensated plot of $N(r)$, the number of cubes of side r containing the scalar fronts satisfying the threshold condition $|\partial\theta/\partial x| \geq 0.2\theta_{\rm rms}/\eta_B$ [26]. Curves are shown for Sc = 8, 32, 128, and 512 for $R_\lambda = 140$. N^3 is the total number of grid points. $D_F = 3 - \zeta_\infty$ is the fractal codimension. We set $D_F = 2$ corresponding to $\zeta_\infty = 1$.

fractal dimension of sharp fronts is the codimension of the saturation exponent of scalar structure functions.

Conclusions.—We have demonstrated by several means that fully developed turbulence, which enabled effective mixing at unity Sc, becomes an ineffective mixer when Sc is large. The scalar-dissipation-rate, when nondimensionalized by large-scale quantities, decreases with Sc and the scalar field effectively oscillates between the largest and smallest concentrations without producing many intermediate levels. We find that the exponents of scalar structure functions saturate for high-order moments; the saturation value appears to be bounded by unity, which is also confirmed by showing that large excursions in $\partial\theta/\partial x$ have a codimension of 2. These results form an important ingredient in a fuller understanding of turbulent mixing, and we note that models like 1D-Burgers equation [41] and Kraichnan's passive scalar [42] have the same behavior of saturated exponents for large moment orders, leveling off at unity.

From a theoretical perspective, our results invite revisions to existing phenomenology of scalar turbulence (for large Sc). While we have considered mixing of passive scalars, it would be instructive to extend these results to active scalars at large Sc, e.g., salinity in the ocean (Sc ~ 700). In oceanic mixing, it is often assumed that the turbulent flux of salinity is equal to that of heat, despite the latter occurring at Sc ~ 7. However, the current study, together with the work of [15], provides strong evidence against it. On a related note, it has been shown in a subsequent analysis [43] that the results reported here are seemingly connected to a Sc correction to the Batchelor length scale, which can play an important role for both passive and active scalars.

---

*dhawal.buaria@nyu.edu

[1] H. Tennekes and J. L. Lumley, *A First Course in Turbulence* (Cambridge, Massachusetts and London, England, 1972).

[2] Z. Warhaft, Passive scalars in turbulent flows, Annu. Rev. Fluid Mech. **32**, 203 (2000).

[3] P. E. Dimotakis, Turbulent mixing, Annu. Rev. Fluid Mech. **37**, 329 (2005).

[4] G. I. Taylor, The statistical theory of turbulence, Proc. R. Soc. A **151**, 421 (1935).

[5] A. N. Kolmogorov, The local structure of turbulence in incompressible viscous fluid for very large Reynolds numbers, Dokl. Akad. Nauk SSSR **30**, 301 (1941).

[6] K. R. Sreenivasan, On the scaling of the turbulence energy dissipation rate, Phys. Fluids **27**, 1048 (1984).

[7] K. R. Sreenivasan, An update on the energy dissipation rate in isotropic turbulence, Phys. Fluids **10**, 528 (1998).

[8] B. Pearson, P.-Å. Krogstad, and W. Van De Water, Measurements of the turbulent energy dissipation rate, Phys. Fluids **14**, 1288 (2002).

[9] Y. Kaneda, T. Ishihara, M. Yokokawa, K. Itakura, and A. Uno, Energy dissipation rate and energy spectrum in high resolution direct numerical simulations of turbulence in a periodic box, Phys. Fluids **15**, L21 (2003).

[10] G. K. Batchelor, Small-scale variation of convected quantities like temperature in turbulent fluid. 1. General discussion and the case of small conductivity, J. Fluid Mech. **5**, 113 (1959).

[11] A. S. Monin and A. M. Yaglom, *Statistical Fluid Mechanics* (MIT Press, Cambridge, MA, 1975), Vol. 2.

[12] B. I. Shraiman and E. D. Siggia, Scalar turbulence, Nature (London) **405**, 639 (2000).

[13] D. A. Donzis, K. R. Sreenivasan, and P. K. Yeung, Scalar dissipation rate and dissipative anomaly in isotropic turbulence, J. Fluid Mech. **532**, 199 (2005).

[14] The case of Sc $\to 0$ is somewhat straightforward and can be expected to yield a similar result as Sc = 1, e.g., see Ref. [13].

[15] J. D. Nash and J. N Moum, Microstructure estimates of turbulent salinity flux and the dissipation spectrum of salinity, J. Phys. Oceanogr. **32**, 2312 (2002).

[16] P. K. Yeung, S. Xu, D. A. Donzis, and K. R. Sreenivasan, Simulations of three-dimensional turbulent mixing for Schmidt numbers of the order 1000, Flow Turbul. Combust. **72**, 333 (2004).

[17] T. Ishihara, T. Gotoh, and Y. Kaneda, Study of high-Reynolds number isotropic turbulence by direct numerical simulations, Annu. Rev. Fluid Mech. **41**, 165 (2009).

[18] D. Buaria, A. Pumir, and E. Bodenschatz, Self-attenuation of extreme events in Navier-Stokes turbulence, Nat. Commun. **11**, 5852 (2020).

[19] P. K. Yeung, S. Xu, and K. R. Sreenivasan, Schmidt number effects on turbulent transport with uniform mean scalar gradient, Phys. Fluids **14**, 4178 (2002).

[20] T. Gotoh, S. Hatanaka, and H. Miura, Spectral compact difference hybrid computation of passive scalar in isotropic turbulence, J. Comput. Phys. **231**, 7398 (2012).

[21] M. P. Clay, D. Buaria, T. Gotoh, and P. K. Yeung, A dual communicator and dual grid-resolution algorithm for petascale simulations of turbulent mixing at high Schmidt number, Comput. Phys. Commun. **219**, 313 (2017).

[22] M. P. Clay, D. Buaria, P. K. Yeung, and T. Gotoh, GPU acceleration of a petascale application for turbulent mixing

at high Schmidt number using OpenMP 4.5, Comput. Phys. Commun. **228,** 100 (2018).

[23] See Supplemental Material at http://link.aps.org/supplemental/10.1103/PhysRevLett.126.074501 for velocity and scalar spectra.

[24] M. P. Clay, Strained turbulence and low-diffusivity turbulent mixing using high performance computing, Ph.D. thesis, Georgia Institute of Technology, 2017.

[25] D. Buaria, A. Pumir, E. Bodenschatz, and P. K. Yeung, Extreme velocity gradients in turbulent flows, New J. Phys. **21,** 043004 (2019).

[26] K. P. Iyer, J. Schumacher, K. R. Sreenivasan, and P. K. Yeung, Steep Cliffs and Saturated Exponents in Three-Dimensional Scalar Turbulence, Phys. Rev. Lett. **121,** 264501 (2018).

[27] D. Buaria, E. Bodenschatz, and A. Pumir, Vortex stretching and enstrophy production in high Reynolds number turbulence, Phys. Rev. Fluids **5,** 104602 (2020).

[28] M. S. Borgas, B. L. Sawford, S. Xu, D. A. Donzis, and P. K. Yeung, High Schmidt number scalars in turbulence: Structure functions and Lagrangian theory, Phys. Fluids **16,** 3888 (2004).

[29] G. Falkovich, K. Gawędzki, and M. Vergassola, Particles and fields in fluid turbulence, Rev. Mod. Phys. **73,** 913 (2001).

[30] K. R. Sreenivasan and J. Schumacher, Lagrangian views on turbulent mixing of passive scalars, Phil. Trans. R. Soc. A **368,** 1561 (2010).

[31] B. L. Sawford and J.-F. Pinton, A Lagrangian view of turbulent dispersion and mixing, in *Ten Chapters in Turbulence*, edited by P. A. Davidson, Y. Kaneda, and K. R. Sreenivasan (Cambridge University Press, Cambridge, England, 2013).

[32] D. Buaria, B. L. Sawford, and P. K. Yeung, Characteristics of backward and forward two-particle relative dispersion in turbulence at different Reynolds numbers, Phys. Fluids **27,** 105101 (2015).

[33] D. Buaria, P. K. Yeung, and B. L. Sawford, A Lagrangian study of turbulent mixing: Forward and backward dispersion of molecular trajectories in isotropic turbulence, J. Fluid Mech. **799,** 352 (2016).

[34] K. R. Sreenivasan, On local isotropy of passive scalars in turbulent shear flows, Proc. R. Soc. A **434,** 165 (1991).

[35] M. Holzer and E. D. Siggia, Turbulent mixing of a passive scalar, Phys. Fluids **6,** 1820 (1994).

[36] A. Celani, A. Lanotte, A. Mazzino, and M. Vergassola, Fronts in passive scalar turbulence, Phys. Fluids **13,** 1768 (2001).

[37] K. R. Sreenivasan, Turbulent mixing: A perspective, Proc. Natl. Acad. Sci. U.S.A. **116,** 18175 (2019).

[38] T. Gotoh and P. K. Yeung, Passive scalar transport in turbulence: A computational perspective, in *Ten Chapters in Turbulence*, edited by P. A. Davidson, Y. Kaneda, and K. R. Sreenivasan (Cambridge University Press, Cambridge, England, 2013).

[39] Although not shown here, we have performed extensive tests (as done in Ref. [26]) to establish statistical convergence of structure functions of high orders.

[40] P. K. Yeung and Y. Zhou, Universality of the Kolmogorov constant in numerical simulations of turbulence, Phys. Rev. E **56,** 1746 (1997).

[41] J. Bec and K. Khanin, Burgers turbulence, Phys. Rep. **447,** 1 (2007).

[42] E. Balkovsky and V. Lebedev, Instanton for the Kraichnan passive scalar problem, Phys. Rev. E **58,** 5776 (1998).

[43] D. Buaria, M. P. Clay, K. R. Sreenivasan, and P. K. Yeung, Small-Scale Isotropy and Ramp-Cliff Structures in Scalar Turbulence, Phys. Rev. Lett. **126,** 034504 (2021).

[44] https://www.gauss-centre.eu.